

Near Capacity Signaling over Fading Channels using Coherent Turbo Coded OFDM and Massive MIMO

K. Vasudevan

Dept. of EE
IIT Kanpur
India

Email: vasu@iitk.ac.in

Abstract—The minimum average signal-to-noise ratio (SNR) per bit required for error-free transmission over a fading channel is derived, and is shown to be equal to that of the additive white Gaussian noise (AWGN) channel, which is -1.6 dB. Discrete-time algorithms are presented for timing and carrier synchronization, as well as channel estimation, for turbo coded multiple input multiple output (MIMO) orthogonal frequency division multiplexed (OFDM) systems. Simulation results show that it is possible to achieve a bit error rate of 10^{-5} at an average SNR per bit of 5.5 dB, using two transmit and two receive antennas. We then propose a near-capacity signaling method in which each transmit antenna uses a different carrier frequency. Using the near-capacity approach, we show that it is possible to achieve a BER of 2×10^{-5} at an average SNR per bit of just 2.5 dB, with one receive antenna for each transmit antenna. When the number of receive antennas for each transmit antenna is increased to 128 , then a BER of 2×10^{-5} is attained at an average SNR per bit of 1.25 dB. In all cases, the number of transmit antennas is two and the spectral efficiency is 1 bit/transmission or 1 bit/sec/Hz. In other words, each transmit antenna sends 0.5 bit/transmission. It is possible to obtain higher spectral efficiency by increasing the number of transmit antennas, with no loss in BER performance, as long as each transmit antenna uses a different carrier frequency. The transmitted signal spectrum for the near-capacity approach can be restricted by pulse-shaping. In all the simulations, a four-state turbo code is used. The corresponding turbo decoder uses eight iterations. The algorithms can be implemented on programmable hardware and there is a large scope for parallel processing.

Keywords—Channel capacity; coherent detection; frequency selective Rayleigh fading channel; massive multiple input multiple output (MIMO); orthogonal frequency division multiplexing (OFDM); spectral efficiency; turbo codes.

I. INTRODUCTION

We begin this article with an open question: what is the operating signal-to-noise (SNR) per bit or E_b/N_0 of the present day mobile phones [1]–[3]? The mobile phones indicate a typical received signal strength of -100 dBm (10^{-10} mW), however this is not the SNR per bit.

The above question assumes significance since future wireless communications, also called the 5th generation or 5G [4]–[7], is supposed to involve not only billions of people, but also smart machines and devices, e.g., driverless cars, remotely controlled washing machines, refrigerators, microwave ovens, robotic surgeries in health care and so on. Thus, we have to

deal with an internet of things (IoT), which involves device-to-human, human-to-device and device-to-device communications. Due to the large number of devices involved, it becomes imperative that each device operates at the minimum possible average SNR per bit required for error-free communication.

Depending on the application, there are different requirements on the communication system. Critical applications like driverless cars and robotic surgeries require low to medium bit rates, e.g., $0.1 - 10$ Mbps and low latency (the time taken to process the received information and send a response back to the transmitter) of the order of a fraction of a millisecond. Some applications like watching movies on a mobile phone require high bit rates, e.g., $10 - 1000$ Mbps for high density and ultra high density (4k) video and can tolerate high latency, of the order of a fraction of a second. Whatever the application, the 5G wireless communication systems are expected to share some common features like having a large number of transmit and receive antennas also called massive multiple input multiple output (MIMO) [8]–[11] and the use of millimeter wave carrier frequencies (> 100 GHz) [12]–[16], to accommodate large bit-rates (> 1 Gbps) and large number of users. In this paper we deal with the physical layer of wireless systems that are also applicable to 5G. The main topics addressed in this work are timing and carrier synchronization, channel estimation, turbo codes and orthogonal frequency division multiplexing (OFDM). Recall that OFDM converts a frequency selective channel into a flat channel [17] [18].

Channel characteristics in the THz frequency range and at 17 GHz for 5G indoor wireless systems is studied in [19] [20]. Channel estimation for massive MIMO assuming spatial correlation between the receive antennas is considered in [21] [22]. In [23], a MIMO channel estimator and beamformer is described. Uplink channel estimation using compressive sensing for millimeter wave, multiuser MIMO systems is considered in [24] [25].

Waveform design for spectral containment of the transmitted signal, is an important aspect of wireless telecommunications, especially in the uplink, where many users access a base station. We require that the signal from one user does not interfere with the other user. This issue is addressed in [26]–[37]. Error control coding for 5G is discussed in [38] [39]. References to carrier and timing synchronization in OFDM can be found in [2] [3] [40].

The capacity of single-user MIMO systems under different

assumptions about the channel impulse response (also called the channel state information or CSI) and the statistics of the channel impulse response (also called channel distribution information or CDI) is discussed in [41]. The capacity of MIMO Rayleigh fading channels in the presence of interference and receive correlation is discussed in [42]. The low SNR capacity of MIMO fading channels with imperfect channel state information is presented in [43].

The main contribution of this paper is to develop discrete-time algorithms for coherently detecting multiple input, multiple output (MIMO), orthogonal frequency division multiplexed (OFDM) signals, transmitted over frequency selective Rayleigh fading channels. Carrier frequency offset and additive white Gaussian noise (AWGN) are the other impairments considered in this work. The minimum SNR per bit required for error-free transmission over frequency selective MIMO fading channels is derived. Finally we demonstrate how we can approach close to the channel capacity.

To the best of our knowledge, other than the work in [40], which deals with turbo coded single input single output (SISO) OFDM, and [2] [3], which deal with turbo coded single input multiple output (SIMO) OFDM, discrete-time algorithms for the coherent detection of turbo coded MIMO OFDM systems have not been discussed earlier in the literature. Coherent detectors for AWGN channels is discussed in [44] [45]. Simulations results for a 2×2 turbo coded MIMO OFDM system indicate that a BER of 10^{-5} , is obtained at an average SNR per bit of just 5.5 dB, which is a 2.5 dB improvement over the performance given in [2]. If each transmit antenna transmits at a different carrier frequency, then we show that it is possible to achieve a BER of 2×10^{-5} at an average SNR per bit of just 2.5 dB, with one receive antenna for each transmit antenna. When the number of receive antennas for each transmit antenna is increased to 128, then a BER of 2×10^{-5} is obtained at an average SNR per bit of 1.25 dB. In all cases, the number of transmit antennas is two and the spectral efficiency is 1 bit/transmission or 1 bit/sec/Hz. In other words, each transmit antenna sends 0.5 bit/transmission. It is possible to obtain higher spectral efficiency by increasing the number of transmit antennas, with no loss in BER performance, as long as each transmit antenna uses a different carrier frequency. It is possible to band limit the transmitted signal using pulse shaping. In all the simulations, a four-state turbo code is used. The corresponding turbo decoder uses eight iterations.

This paper is organized as follows. Section II presents the system model. The discrete-time algorithms and simulation results for the coherent receiver are given in Section III. Near-capacity signaling is presented in Section IV. Finally, Section V concludes the paper.

II. SYSTEM MODEL

We assume a MIMO-OFDM system with N_t transmit and N_r receive antennas, with QPSK modulation. The data from each transmit antenna is organized into frames, as shown in Figure 1(a), similar to [2] [3] [40]. Note the presence of the cyclic suffix, whose purpose will be explained later. In Figure 1(b), we observe that only the data and postamble QPSK symbols are interleaved. The buffer QPSK symbols (B) are sent to the IFFT without interleaving. In Figure 1, the

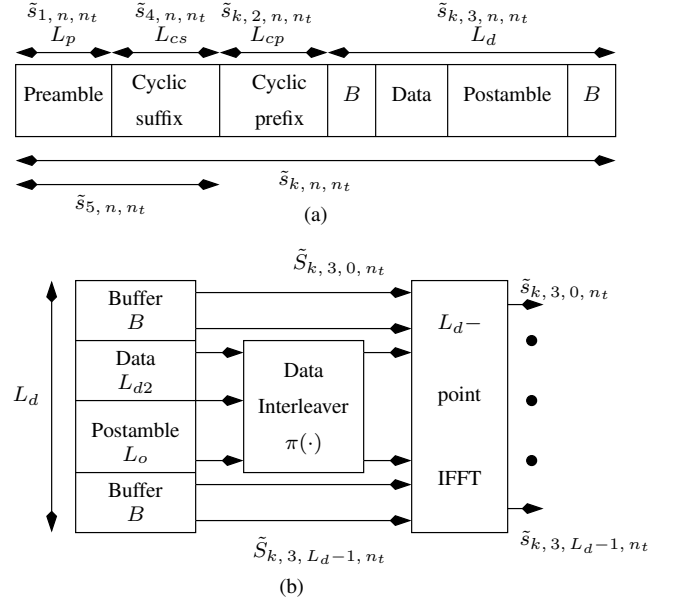


Figure 1. The frame structure in the time domain.

subscript k refers to the k^{th} frame, n denotes the time index in a frame and $1 \leq n_t \leq N_t$ is the index to the transmit antenna. The total length of the frame is

$$L = L_p + L_{cs} + L_{cp} + L_d. \quad (1)$$

Let us assume a channel span equal to L_h . The channel span assumed by the receiver is [3] [40]

$$L_{hr} = 2L_h - 1 \quad (2)$$

Note that L_h depends on the delay spread of the channel, and is measured in terms of the number of symbols. Recall that, the delay spread is a measure of the time difference between the arrival of the first and the last multipath signal, as seen by the receiver. Typically

$$L_h = d_0 / (cT_s) \quad (3)$$

where d_0 is the distance between the longest and shortest multipath, c is the velocity of light and T_s is the symbol duration which is equal to the sample spacing of \tilde{s}_{k,n,n_t} in Figure 1(a). We have assumed a situation where the mobile is close to the base station and the longest path is reflected from the cell edge, which is approximately equal to the cell diameter d_0 , as shown in Figure 2. The base stations, depicted by green dots, are interconnected by a high data-rate backhaul, shown by the blue lines. The cell edge is given by the red circles. Note that $d_1 < d_0$. In order to obtain symmetry, the backhaul forms an equilateral triangle of length d_1 . The base station is at the center of each cell, whose diameter is d_0 . For $L_h = 10$, $1/T_s = 10^7$ bauds and $c = 3 \times 10^8$ meters per sec, we get $d_0 = 300$ meters. Similarly with $L_h = 10$ and $1/T_s = 10^8$ bauds we obtain $d_0 = 30$ meters. In other words, as the baud rate increases, the cell size needs to decrease, and consequently the transmit power decreases, for the same channel span L_h . The length of the cyclic prefix and suffix is [17]:

$$L_{cp} = L_{cs} = L_{hr} - 1. \quad (4)$$

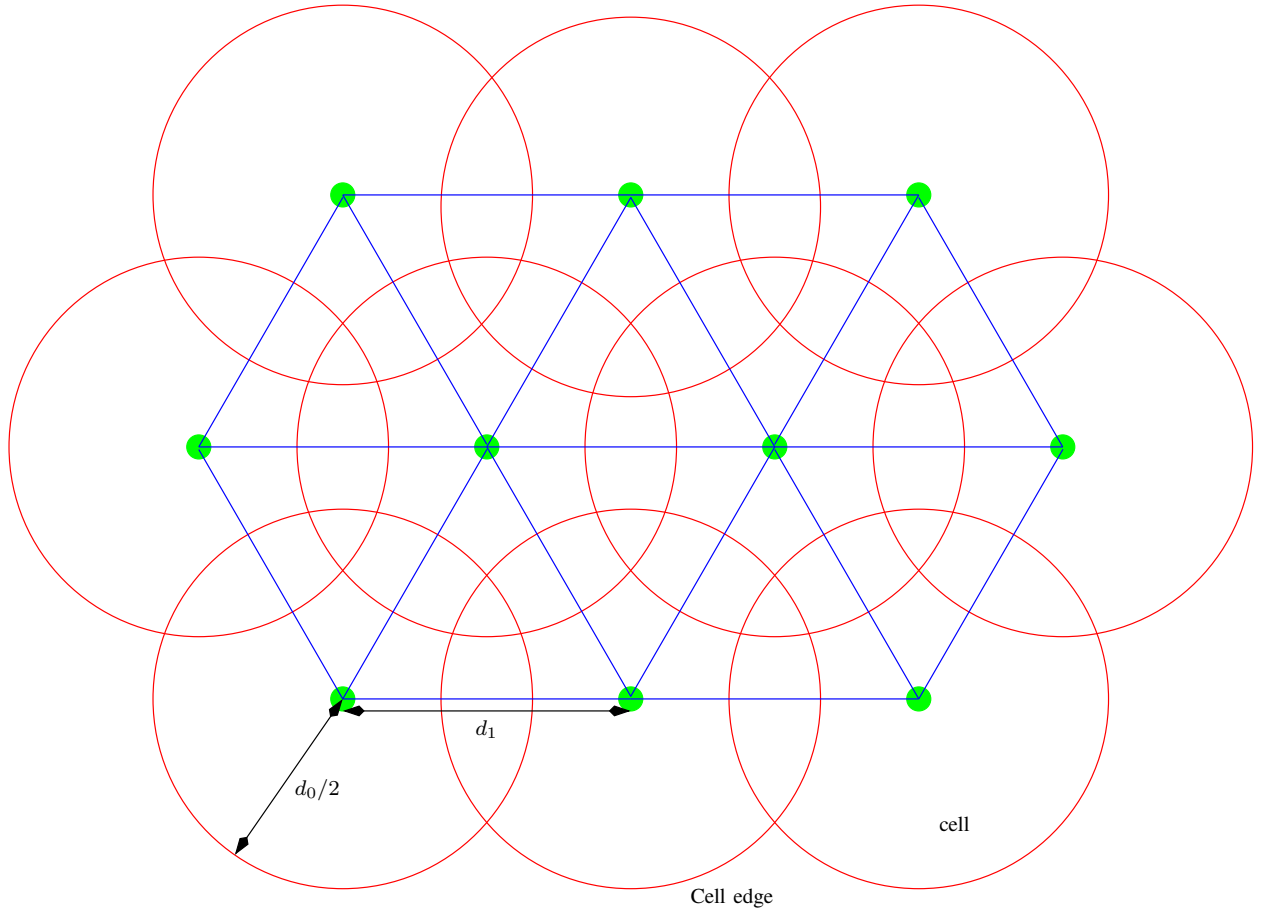


Figure 2. Arrangement of cells and base stations.

Throughout the manuscript, we use tilde to denote complex quantities. However, complex QPSK symbols will be denoted without a tilde, e.g., S_{1,n,n_t} . Boldface letters denote vectors or matrices. The channel coefficients \tilde{h}_{k,n,n_r,n_t} associated with the receive antenna n_r ($1 \leq n_r \leq N_r$) and transmit antenna n_t ($1 \leq n_t \leq N_t$) for the k^{th} frame are $\mathcal{CN}(0, 2\sigma_f^2)$ and independent over time n , that is:

$$\frac{1}{2}E \left[\tilde{h}_{k,n,n_r,n_t} \tilde{h}_{k,n-m,n_r,n_t}^* \right] = \sigma_f^2 \delta_K(m) \quad (5)$$

where “*” denotes complex conjugate and $\delta_K(\cdot)$ is the Kronecker delta function. This implies a uniform power delay profile. Note that even though an exponential power delay profile is more realistic, we have used a uniform power delay profile, since it is expected to give the worst-case BER performance, as all the multipath components have the same power. The channel is assumed to be quasi-static, that is \tilde{h}_{k,n,n_r,n_t} is time-invariant over one frame and varies independently from frame-to-frame, as given by:

$$\frac{1}{2}E \left[\tilde{h}_{k,n,n_r,n_t} \tilde{h}_{j,n,n_r,n_t}^* \right] = \sigma_f^2 \delta_K(k-j) \quad (6)$$

where k and j denote the frame indices.

The AWGN noise samples \tilde{w}_{k,n,n_r} for the k^{th} frame at time n and receive antenna n_r are $\mathcal{CN}(0, 2\sigma_w^2)$. The frequency offset ω_k for the k^{th} frame is uniformly distributed

over $[-0.04, 0.04]$ radian [46]. We assume that ω_k is fixed for a frame and varies randomly from frame-to-frame.

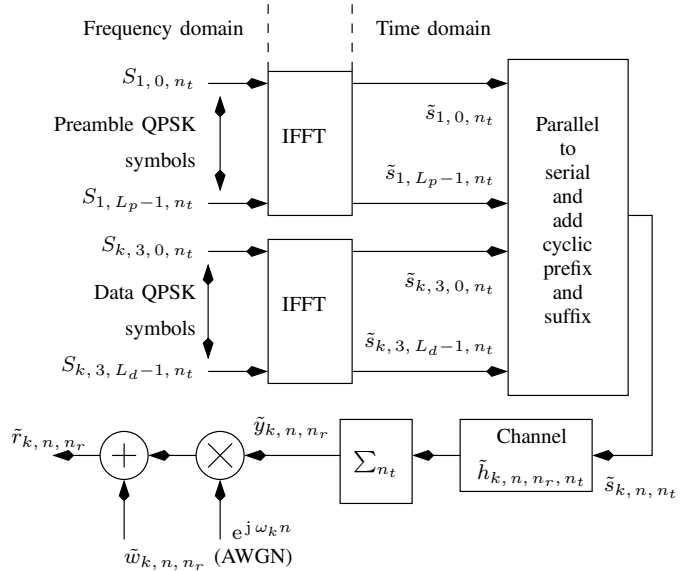


Figure 3. Block diagram of the transmitter.

The block diagram of the transmitter is given in Figure 3.

With reference to Figs. 1(a) and 3, note that:

$$\begin{aligned}
\tilde{s}_{1,n,n_t} &= \frac{1}{L_p} \sum_{i=0}^{L_p-1} S_{1,i,n_t} e^{j2\pi ni/L_p} \\
&\quad \text{for } 0 \leq n \leq L_p - 1 \\
\tilde{s}_{k,3,n,n_t} &= \frac{1}{L_d} \sum_{i=0}^{L_d-1} S_{k,3,i,n_t} e^{j2\pi ni/L_d} \\
&\quad \text{for } 0 \leq n \leq L_d - 1 \\
\tilde{s}_{k,2,n,n_t} &= \tilde{s}_{k,3,L_d-L_{cp}+n,n_t} \\
&\quad \text{for } 0 \leq n \leq L_{cp} - 1 \\
\tilde{s}_{4,n,n_t} &= \tilde{s}_{1,n,n_t} \\
&\quad \text{for } 0 \leq n \leq L_{cs} - 1 \\
\tilde{s}_{5,n,n_t} &= \tilde{s}_{1,n,n_t} + \tilde{s}_{4,n-L_p,n_t}. \tag{7}
\end{aligned}$$

From (7), it is clear that the preamble is independent of the frame k . However, each transmit antenna has its own preamble, for the purpose of synchronization and channel estimation at the receiver.

The preamble in the frequency domain, for each transmit antenna is generated as follows. Let $\pi_p(i)$, for $0 \leq i \leq L_p - 1$, denote the interleaver map for the preamble. Let

$$\mathbf{S}_r = [S_{r,0} \quad \dots \quad S_{r,L_p-1}]_{L_p \times 1}^T \tag{8}$$

denote a random vector of QPSK symbols. The preamble vector for the transmit antenna n_t is first initialized by

$$\begin{aligned}
\mathbf{S}_{1,n_t} &= [S_{1,0,n_t} \quad \dots \quad S_{1,L_p-1,n_t}]_{L_p \times 1}^T \\
&= \mathbf{0}_{L_p \times 1}. \tag{9}
\end{aligned}$$

Next, we substitute

$$\mathbf{S}_{1,\pi_p(i_4:i_5),n_t} = \mathbf{S}_r(i_4:i_5). \tag{10}$$

where $i_4:i_5$ denotes the range of indices from i_4 to i_5 , both inclusive, and

$$\begin{aligned}
i_4 &= (n_t - 1)L_p/N_t \\
i_5 &= i_4 + L_p/N_t - 1. \tag{11}
\end{aligned}$$

Note that the preamble in the frequency domain for each transmit antenna has only L_p/N_t non-zero elements, the rest of the elements are zero. Moreover, due to $\pi_p(\cdot)$, the L_p/N_t non-zero elements are randomly interspersed over the L_p subcarriers in the frequency domain, for each transmit antenna.

By virtue of the preamble construction in (9), (10) and (11), the preambles in the frequency and time domains corresponding to transmit antennas n_t and m_t satisfy the relation (using Parseval's energy theorem):

$$\begin{aligned}
S_{1,i,n_t} S_{1,i,m_t}^* &= (2N_t L_p / L_d) \delta_K(n_t - m_t) \\
&\quad \text{for } 0 \leq i \leq L_p - 1 \\
\Rightarrow \tilde{s}_{1,n,n_t} \odot_{L_p} \tilde{s}_{1,-n,m_t}^* &= \begin{cases} 0 & \text{for } n_t \neq m_t, \\ (2L_p/L_d) \delta_K(n) & 0 \leq n \leq L_p - 1 \\ & \text{for } n_t = m_t \end{cases} \tag{12}
\end{aligned}$$

where " \odot_{L_p} " denotes the L_p -point circular convolution. In other words, the preambles corresponding to distinct transmit antennas are orthogonal over L_p samples. Moreover, the autocorrelation of the preambles in frequency and time domain,

can be approximated by a weighted Kronecker delta function (this condition is usually satisfied by random sequences having zero-mean; the approximation gets better as L_p increases).

We assume $S_{k,3,i,n_t} \in \{\pm 1 \pm j\}$. Since we require:

$$E \left[|\tilde{s}_{1,n,n_t}|^2 \right] = E \left[|\tilde{s}_{k,3,n,n_t}|^2 \right] = 2/L_d \triangleq \sigma_s^2 \tag{13}$$

we must have $S_{1,i,n_t} \in \sqrt{L_p N_t / L_d} (\pm 1 \pm j)$. In other words, the average power of the preamble part must be equal to the average power of the data part, in the time domain.

Due to the presence of the cyclic suffix in Figure 1 and (7), and due to (12), we have

$$\begin{aligned}
\tilde{s}_{5,n,n_t} \star \tilde{s}_{1,L_p-1-n,m_t}^* &= \begin{cases} 0 & \text{for } L_p - 1 \leq n \leq L_p + L_{hr} - 2, \\ & n_t \neq m_t \\ (2L_p/L_d) \delta_K(n - L_p + 1) & \text{for } n_t = m_t \end{cases} \tag{14}
\end{aligned}$$

where " \star " denotes linear convolution.

The signal for the k^{th} frame and receive antenna n_r can be written as (for $0 \leq n \leq L + L_h - 2$):

$$\begin{aligned}
\tilde{r}_{k,n,n_r} &= \sum_{n_t=1}^{N_t} \left(\tilde{s}_{k,n,n_t} \star \tilde{h}_{k,n,n_r,n_t} \right) e^{j\omega_k n} + \tilde{w}_{k,n,n_r} \\
&= \tilde{y}_{k,n,n_r} e^{j\omega_k n} + \tilde{w}_{k,n,n_r} \tag{15}
\end{aligned}$$

where \tilde{s}_{k,n,n_t} is depicted in Figure 1(a) and

$$\tilde{y}_{k,n,n_r} = \sum_{n_t=1}^{N_t} \tilde{s}_{k,n,n_t} \star \tilde{h}_{k,n,n_r,n_t}. \tag{16}$$

Note that any random carrier phase can be absorbed in the channel impulse response.

The uplink and downlink transmissions between the mobiles and base station could be carried out using time division duplex (TDD) or frequency division duplex (FDD). Time division (TDMA), frequency division (FDMA), code division (CDMA), orthogonal frequency division (OFDMA), for downlink transmissions and filterbank multicarrier (FBMC), for uplink transmissions [26], are the possible choices for multiple access (MA) techniques.

III. RECEIVER

In this section, we discuss the discrete-time receiver algorithms.

A. Start of Frame (SoF) and Coarse Frequency Offset Estimate

The start of frame (SoF) detection and coarse frequency offset estimation is performed for each receive antenna $1 \leq n_r \leq N_r$ and transmit antenna $1 \leq n_t \leq N_t$, as given by the following rule (similar to (22) in [40] and (24) in [3]): choose that value of m and ν_k which maximizes

$$\left| \left(\tilde{r}_{k,m,n_r} e^{-j\nu_k m} \right) \star \tilde{s}_{1,L_p-1-m,n_t}^* \right|. \tag{17}$$

Let $\hat{m}_k(\cdot)$ denote the time instant and $\hat{\nu}_k(\cdot)$ denote the coarse estimate of the frequency offset (both of which are functions of n_r and n_t), at which the maximum in (17) is obtained. Note

that (17) is a two-dimensional search over m and ν_k , which can be efficiently implemented in hardware, and there is a large scope for parallel processing. In particular, the search over ν_k involves dividing the range of ω_k ($[-0.04, 0.04]$ radians) into B_1 frequency bins, and deciding in favour of that bin which maximizes (17). In our simulations, $B_1 = 64$ [3] [40].

Note that in the absence of noise and due to the properties given in (14)

$$\hat{m}_k(n_r, n_t) = L_p - 1 + \operatorname{argmax}_m \left| \tilde{h}_{k,m,n_r,n_t} \right| \quad (18)$$

where argmax_m corresponds to the value of m for which $\left| \tilde{h}_{k,m,n_r,n_t} \right|$ is maximum. We also have

$$L_p - 1 \leq \hat{m}_k(n_r, n_t) \leq L_p + L_h - 2. \quad (19)$$

If $\hat{m}_k(\cdot)$ lies outside the range in (19), the frame is declared as erased (not detected). This implies that the peak in (17) is due to noise, and not due to the channel. The results for SoF detection at 0 dB SNR per bit for $L_p = 512, 1024, 4096$ are given in Figs. 4, 5, and 6, respectively, for $N_t = N_r = 2$. The parameter Z in the three figures denotes the correlation magnitude given by (17).

The average value of the coarse frequency offset estimate is given by

$$\hat{\omega}_k = \frac{\sum_{n_r=1}^{N_r} \sum_{n_t=1}^{N_t} \hat{\nu}_k(n_r, n_t)}{N_r N_t}. \quad (20)$$

B. Channel Estimation

We assume that the SoF has been estimated using (17) with outcome $m_{0,k}$ given by (assuming the condition in (19) is satisfied for all n_r and n_t):

$$m_{0,k} = \hat{m}_k(1, 1) - L_p + 1 \quad 0 \leq m_{0,k} \leq L_h - 1 \quad (21)$$

and the frequency offset has been perfectly canceled [3] [40]. Observe that any value of n_r and n_t can be used in the computation of (21). We have taken $n_r = n_t = 1$. Define

$$m_{1,k} = m_{0,k} + L_h - 1. \quad (22)$$

For the sake of notational simplicity, we drop the subscript k in $m_{1,k}$, and refer to it as m_1 . The steady-state, preamble part of the received signal for the k^{th} frame and receive antenna n_r can be written as:

$$\tilde{\mathbf{r}}_{k,m_1,n_r} = \sum_{n_t=1}^{N_t} \tilde{\mathbf{s}}_{5,n_t} \tilde{\mathbf{h}}_{k,n_r,n_t} + \tilde{\mathbf{w}}_{k,m_1,n_r} \quad (23)$$

where

$$\begin{aligned} \tilde{\mathbf{r}}_{k,m_1,n_r} &= \begin{bmatrix} \tilde{r}_{k,m_1,n_r} & \cdots & \tilde{r}_{k,m_1+L_p-1,n_r} \end{bmatrix}^T \\ &\quad [L_p \times 1] \text{ vector} \\ \tilde{\mathbf{w}}_{k,m_1,n_r} &= \begin{bmatrix} \tilde{w}_{k,m_1,n_r} & \cdots & \tilde{w}_{k,m_1+L_p-1,n_r} \end{bmatrix}^T \\ &\quad [L_p \times 1] \text{ vector} \\ \tilde{\mathbf{h}}_{k,n_r,n_t} &= \begin{bmatrix} \tilde{h}_{k,0,n_r,n_t} & \cdots & \tilde{h}_{k,L_h-1,n_r,n_t} \end{bmatrix}^T \\ &\quad [L_h \times 1] \text{ vector} \\ \tilde{\mathbf{s}}_{5,n_t} &= \begin{bmatrix} \tilde{s}_{5,L_h-1,n_t} & \cdots & \tilde{s}_{5,0,n_t} \\ \vdots & \cdots & \vdots \\ \tilde{s}_{5,L_p+L_h-2,n_t} & \cdots & \tilde{s}_{5,L_p-1,n_t} \end{bmatrix} \\ &\quad [L_p \times L_h] \text{ matrix} \end{aligned} \quad (24)$$

where L_{hr} is the channel length assumed by the receiver (see (2)), $\tilde{\mathbf{s}}_{5,n_t}$ is the channel estimation matrix and $\tilde{\mathbf{r}}_{k,m_1,n_r}$ is the received signal vector *after* cancellation of the frequency offset. Observe that $\tilde{\mathbf{s}}_{5,n_t}$ is independent of m_1 and due to the relations in (12) and (14), we have

$$\tilde{\mathbf{s}}_{5,m_t}^H \tilde{\mathbf{s}}_{5,n_t} = \begin{cases} \mathbf{0}_{L_{hr} \times L_{hr}} & \text{for } n_t \neq m_t \\ (2L_p/L_d) \mathbf{I}_{L_{hr}} & \text{for } n_t = m_t \end{cases} \quad (25)$$

where $\mathbf{I}_{L_{hr}}$ is an $L_{hr} \times L_{hr}$ identity matrix and $\mathbf{0}_{L_{hr} \times L_{hr}}$ is an $L_{hr} \times L_{hr}$ null matrix. The statement of the ML channel estimation is as follows. Find $\hat{\mathbf{h}}_{k,n_r,m_t}$ (the estimate of $\tilde{\mathbf{h}}_{k,n_r,m_t}$) such that:

$$\begin{aligned} &\left(\tilde{\mathbf{r}}_{k,m_1,n_r} - \sum_{m_t=1}^{N_t} \tilde{\mathbf{s}}_{5,m_t} \hat{\mathbf{h}}_{k,n_r,m_t} \right)^H \\ &\left(\tilde{\mathbf{r}}_{k,m_1,n_r} - \sum_{m_t=1}^{N_t} \tilde{\mathbf{s}}_{5,m_t} \hat{\mathbf{h}}_{k,n_r,m_t} \right) \end{aligned} \quad (26)$$

is minimized. Differentiating with respect to $\hat{\mathbf{h}}_{k,n_r,m_t}^*$ and setting the result to zero yields [17] [47]:

$$\hat{\mathbf{h}}_{k,n_r,m_t} = (\tilde{\mathbf{s}}_{5,m_t}^H \tilde{\mathbf{s}}_{5,m_t})^{-1} \tilde{\mathbf{s}}_{5,m_t}^H \tilde{\mathbf{r}}_{k,m_1,n_r}. \quad (27)$$

Observe that when $m_{0,k} = L_h - 1$ in (21), and noise is absent (see (29) in [40] and (35) in [3]), we obtain:

$$\begin{aligned} &\hat{\mathbf{h}}_{k,n_r,m_t} \\ &= \begin{bmatrix} \tilde{h}_{k,0,n_r,m_t} & \cdots & \tilde{h}_{k,L_h-1,n_r,m_t} & 0 & \cdots & 0 \end{bmatrix}^T. \end{aligned} \quad (28)$$

Similarly, when $m_{0,k} = 0$ and in the absence of noise:

$$\begin{aligned} &\hat{\mathbf{h}}_{k,n_r,m_t} \\ &= \begin{bmatrix} 0 & \cdots & 0 & \tilde{h}_{k,0,n_r,m_t} & \cdots & \tilde{h}_{k,L_h-1,n_r,m_t} \end{bmatrix}^T. \end{aligned} \quad (29)$$

To see the effect of noise on the channel estimate in (27), consider

$$\tilde{\mathbf{u}} = (\tilde{\mathbf{s}}_{5,m_t}^H \tilde{\mathbf{s}}_{5,m_t})^{-1} \tilde{\mathbf{s}}_{5,m_t}^H \tilde{\mathbf{w}}_{k,m_1,n_r}. \quad (30)$$

It can be shown that

$$E[\tilde{\mathbf{u}}\tilde{\mathbf{u}}^H] = \frac{\sigma_w^2 L_d}{L_p} \mathbf{I}_{L_{hr}} \triangleq 2\sigma_u^2 \mathbf{I}_{L_{hr}}. \quad (31)$$

Therefore, the variance of the ML channel estimate (σ_u^2) tends to zero as $L_p \rightarrow \infty$ and L_d is kept fixed. Conversely, when L_d is increased keeping L_p fixed, there is noise enhancement [2] [3]. The magnitude spectrum of the actual and estimated channel for various preamble lengths are shown in Figs. 7, 8 and 9 for $N_t = N_r = 2$ and 0 dB average SNR per bit. Note that \tilde{H}_{k,i,n_r,n_t} denotes the L_d -point discrete Fourier transform (DFT) of \tilde{h}_{k,n,n_r,n_t} in (5).

C. Fine Frequency Offset Estimation

The fine frequency offset estimate is obtained using the following rule: choose that value of time instant m and frequency offset $\nu_{k,f}$ which maximizes:

$$\left| \left(\tilde{r}_{k,m,n_r} e^{-j(\hat{\omega}_k + \nu_{k,f})m} \right) \star \tilde{y}_{1,k,L_2-1-m,n_r,n_t}^* \right| \quad (32)$$

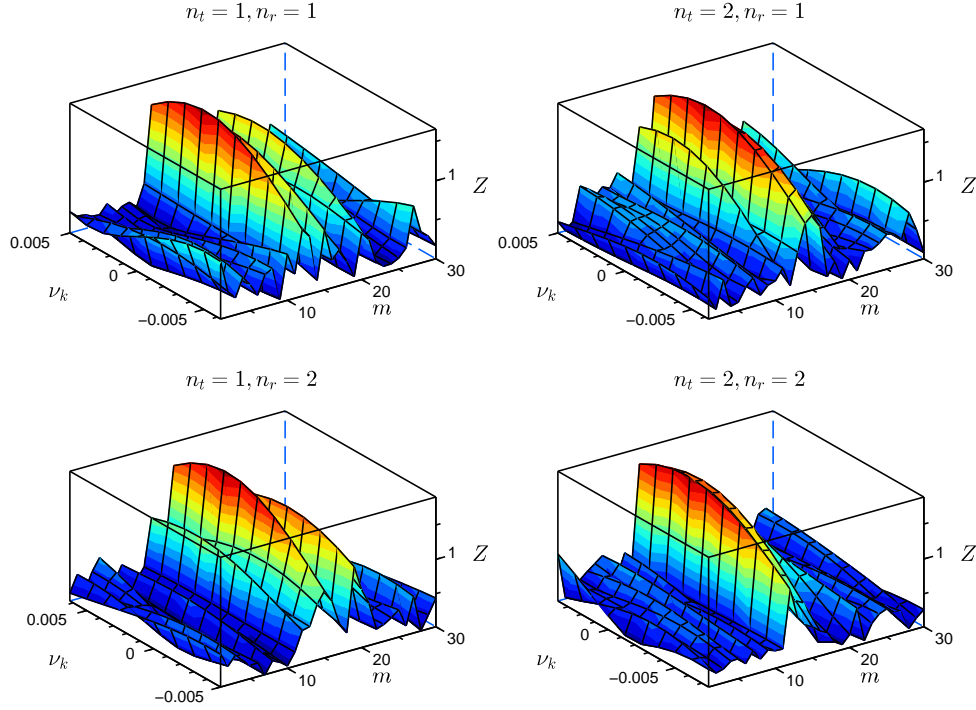


Figure 4. SoF detection at 0 dB SNR per bit, $L_p = 512$.

where

$$\begin{aligned} L_2 &= L_{hr} + L_p - 1 \\ \hat{y}_{1,k,m,n_r,n_t} &= \tilde{s}_{1,m,n_t} \star \hat{h}_{k,m,n_r,n_t} \end{aligned} \quad (33)$$

where \hat{h}_{k,m,n_r,n_t} is obtained from (27). The fine frequency offset estimate ($\hat{\nu}_{k,f}(n_r, n_t)$) is obtained by dividing the interval $[\hat{\omega}_k - 0.005, \hat{\omega}_k + 0.005]$ radian ($\hat{\omega}_k$ is given in (20)) into $B_2 = 64$ frequency bins [44]. The reason for choosing 0.005 radian can be traced to Figure 5 of [3]. We find that the maximum error in the coarse estimate of the frequency offset is approximately 0.004 radian over 10^4 frames. Thus the probability that the maximum error exceeds 0.005 radian is less than 10^{-4} . However, from Table IV in this paper, we note that the maximum error in the frequency offset is 2.4×10^{-2} radians for $L_p = 512$, and 1.1×10^{-2} for $L_p = 1024$, both of which are larger than 0.005 radian. By observing this trend, we expect that for larger values of L_p , say $L_p = 4096$, the maximum error in the coarse frequency offset estimate would be less than 0.005 radians. Increasing L_p would also imply an increase in L_d , for the same throughput (see (54)). The average value of the fine frequency offset estimate is given by:

$$\hat{\omega}_{k,f} = \frac{\sum_{n_r=1}^{N_r} \sum_{n_t=1}^{N_t} \hat{\nu}_{k,f}(n_r, n_t)}{N_r N_t}. \quad (34)$$

D. Super Fine Frequency Offset Estimation

The fine frequency offset estimate in (34) is still inadequate for turbo decoding and data detection when $L_d \gg L_p$ [40]. Note that the residual frequency offset is equal to:

$$\omega_k - \hat{\omega}_k - \hat{\omega}_{k,f}. \quad (35)$$

This residual frequency offset is estimated by interpolating the FFT output and performing postamble matched filtering at the receiver [2] [3]. If the interpolation factor is I , then the FFT size is IL_d (interpolation in the frequency domain is achieved by zero-padding the FFT input in the time domain, and then taking the IL_d -point FFT). Let

$$m_{2,k} = m_{1,k} + L_p + L_{cs} \quad (36)$$

where $m_{1,k}$ is defined in (22). Once again, we drop the subscript k from $m_{2,k}$ and refer to it as m_2 . Define the FFT input in the time domain as:

$$\tilde{\mathbf{r}}_{k,m_2,n_r} = [\tilde{r}_{k,m_2,n_r} \ \dots \ \tilde{r}_{k,m_2+L_d-1,n_r}]^T \quad (37)$$

which is the data part of the received signal in (15) for the k^{th} frame and receive antenna n_r , assumed to have the residual frequency offset given by (35). The output of the IL_d -point FFT of $\tilde{\mathbf{r}}_{k,m_2,n_r}$ in (37) is denoted by

$$\tilde{R}_{k,i,n_r} = \sum_{n=0}^{L_d-1} \tilde{r}_{k,m_2+n,n_r} e^{-j2\pi in/(IL_d)} \quad (38)$$

for $0 \leq i \leq IL_d - 1$.

The coefficients of the postamble matched filter is obtained as follows [2] [3]. Define

$$\tilde{G}_{k,i,n_r}'' = \sum_{n_t=1}^{N_t} \hat{H}_{k,i_3,n_r,n_t} S_{k,3,i,n_t} \quad \text{for } i_0 \leq i \leq i_1 \quad (39)$$

where \hat{H}_{k,i,n_r,n_t} is the L_d -point FFT of the channel estimate

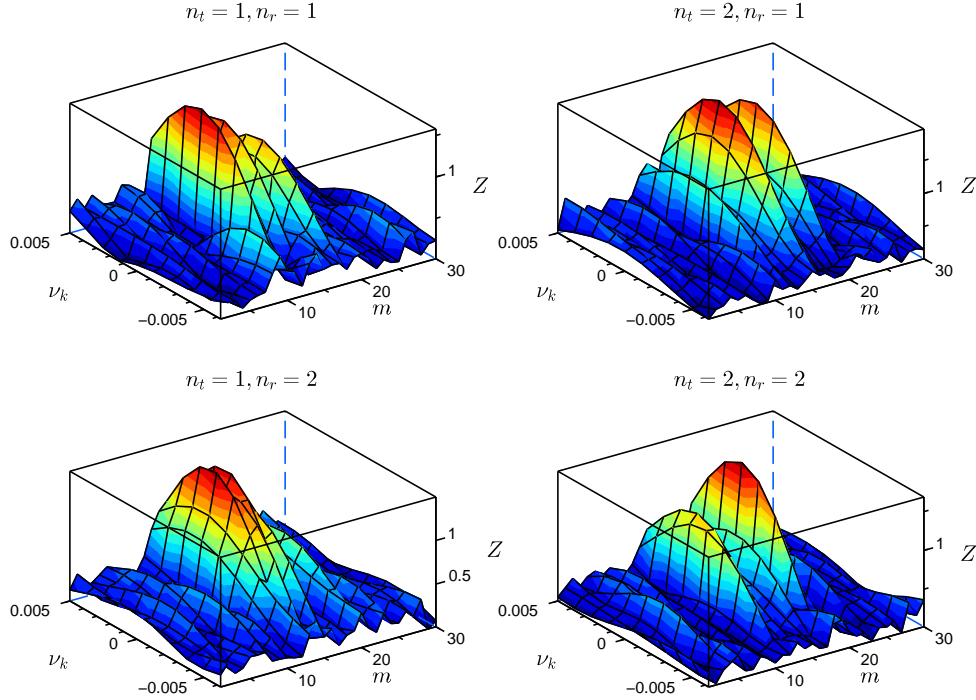


Figure 5. SoF detection at 0 dB SNR per bit, $L_p = 1024$.

in (27), and

$$\begin{aligned} i_0 &= B + L_{d2} \\ i_1 &= i_0 + L_o - 1 \\ i_3 &= B + \pi(i - B) \end{aligned} \quad (40)$$

where $\pi(\cdot)$ is the data interleaver map, B , L_{d2} and L_o are the lengths of the buffer, data, and postamble, respectively, as shown in Figure 1(b). Let

$$\tilde{G}'_{k, i_3, n_r} = \begin{cases} \tilde{G}''_{k, i, n_r} & \text{for } i_0 \leq i \leq i_1 \\ 0 & \text{otherwise} \end{cases} \quad (41)$$

where $0 \leq i_3 \leq L_d - 1$, the relation between i_3 and i is given in (40). Next, we perform interpolation:

$$\tilde{G}_{k, i_4, n_r} = \begin{cases} \tilde{G}'_{k, i, n_r} & \text{for } 0 \leq i \leq L_d - 1 \\ 0 & \text{otherwise} \end{cases} \quad (42)$$

where $0 \leq i_4 \leq IL_d - 1$ and $i_4 = iI$. Finally, the postamble matched filter is $\tilde{G}_{k, IL_d - 1 - i, n_r}^*$, which is convolved with \tilde{R}_{k, i, n_r} in (38). Note that due to the presence of the cyclic prefix, any residual frequency offset in the time domain, manifests as a circular shift in the frequency domain. The purpose of the postamble matched filter is to capture this shift. The role of the buffer symbols is explained in [2] [3]. Assume that the peak of the postamble matched filter output occurs at $m_{3, k}(n_r)$. Ideally, in the absence of noise and frequency offset

$$m_{3, k}(n_r) = IL_d - 1. \quad (43)$$

In the presence of the frequency offset, the peak occurs to the left or right of $IL_d - 1$. The average superfine estimate of the

residual frequency offset is given by:

$$\hat{\omega}_{k, sf} = 2\pi / (IL_d N_r) \sum_{n_r=1}^{N_r} [m_{3, k}(n_r) - IL_d + 1]. \quad (44)$$

E. Noise Variance Estimation

The noise variance is estimated as follows, for the purpose of turbo decoding:

$$\hat{\sigma}_w^2 = \frac{1}{2L_p N_r} \sum_{n_r=1}^{N_r} \left(\tilde{\mathbf{r}}_{k, m_1, n_r} - \sum_{n_t=1}^{N_t} \tilde{\mathbf{s}}_{5, n_t} \hat{\mathbf{h}}_{k, n_r, n_t} \right)^H \left(\tilde{\mathbf{r}}_{k, m_1, n_r} - \sum_{n_t=1}^{N_t} \tilde{\mathbf{s}}_{5, n_t} \hat{\mathbf{h}}_{k, n_r, n_t} \right). \quad (45)$$

F. Turbo Decoding

In this section, we assume that the frequency offset has been perfectly canceled, that is, $\tilde{\mathbf{r}}_{k, m_2, n_r}$ in (37) contains no frequency offset. The output of the L_d -point FFT of $\tilde{\mathbf{r}}_{k, m_2, n_r}$ for the k^{th} frame is given by:

$$\tilde{R}_{k, i, n_r} = \sum_{n_t=1}^{N_t} \tilde{H}_{k, i, n_r, n_t} S_{k, 3, i, n_t} + \tilde{W}_{k, i, n_r} \quad (46)$$

for $0 \leq i \leq L_d - 1$, where $\tilde{H}_{k, i, n_r, n_t}$ is the L_d -point FFT of $\tilde{h}_{k, i, n_r, n_t}$ and \tilde{W}_{k, i, n_r} is the L_d -point FFT of \tilde{w}_{k, i, n_r} . It can be shown that [3] [40]

$$\begin{aligned} \frac{1}{2} E \left[\left| \tilde{W}_{k, i, n_r} \right|^2 \right] &= L_d \sigma_w^2 \\ \frac{1}{2} E \left[\left| \tilde{H}_{k, i, n_r, n_t} \right|^2 \right] &= L_h \sigma_f^2. \end{aligned} \quad (47)$$

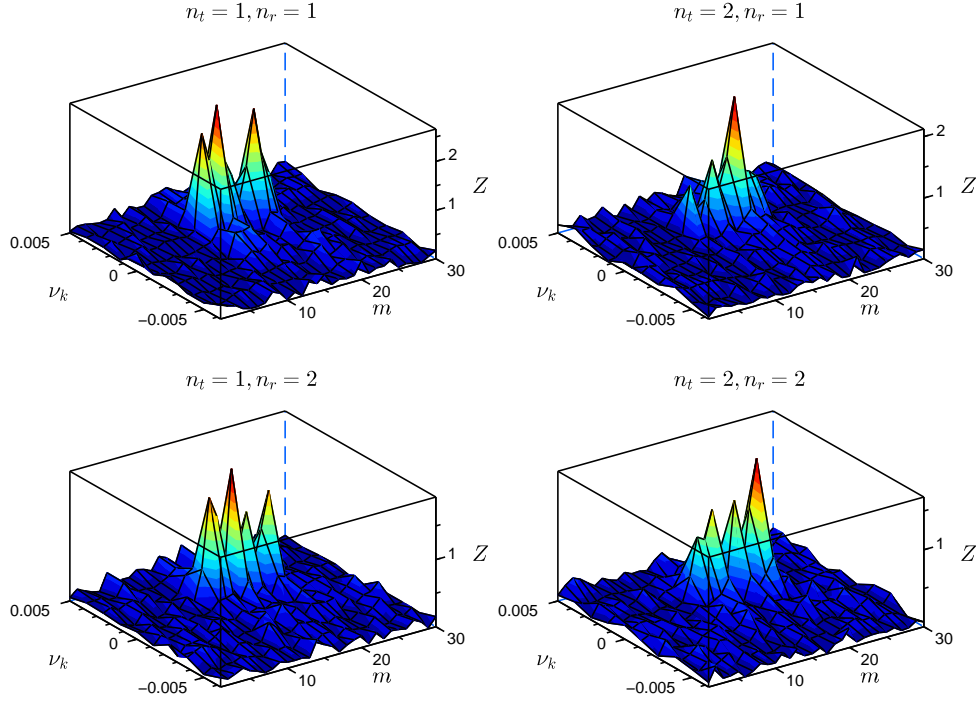


Figure 6. SoF detection at 0 dB SNR per bit, $L_p = 4096$.

The received signal in (46), for the k^{th} frame and i^{th} subcarrier, can be written in matrix form as follows:

$$\tilde{\mathbf{R}}_{k,i} = \tilde{\mathbf{H}}_{k,i} \mathbf{S}_{k,3,i} + \tilde{\mathbf{W}}_{k,i} \quad (48)$$

where $\tilde{\mathbf{R}}_{k,i}$ is the $N_r \times 1$ received signal vector, $\tilde{\mathbf{H}}_{k,i}$ is the $N_r \times N_t$ channel matrix, $\mathbf{S}_{k,3,i}$ is the $N_t \times 1$ symbol vector and $\tilde{\mathbf{W}}_{k,i}$ is the $N_r \times 1$ noise vector.

The generating matrix of each of the constituent encoders is given by (41) in [3], and is repeated here for convenience:

$$\mathbf{G}(D) = \begin{bmatrix} 1 & \frac{1+D^2}{1+D+D^2} \end{bmatrix}. \quad (49)$$

For the purpose of turbo decoding, we consider the case where $N_r = N_t = 2$. The details of turbo decoding can be found in [3], and will not be discussed here. Suffices to say that corresponding to the transition from state m to state n , at decoder 1, for the k^{th} frame, at time i , we define (for $0 \leq i \leq L_{d2} - 1$):

$$\gamma_{1,k,i,m,n} = \exp(-Z_{1,k,i,m,n} / (2L_d \hat{\sigma}_w^2)) \quad (50)$$

where $Z_{1,k,i,m,n}$ is given by

$$\min_{\text{all } S_{m,n,2}} \sum_{n_r=1}^2 \left| \tilde{R}_{k,i,n_r} - \sum_{n_t=1}^2 \hat{H}_{k,i,n_r,n_t} S_{m,n,n_t} \right|^2 \quad (51)$$

where S_{m,n,n_t} denotes the QPSK symbol corresponding to the transition from state m to state n in the trellis, at transmit antenna n_t . Observe that $\hat{\sigma}_w^2$ is the estimate of σ_w^2 obtained from (45). Observe that the minimization in (51) is over all possible QPSK symbols, at $n_t = 2$ and index i . Similarly, for

the transition from state m to state n , at decoder 2, for the k^{th} frame, at time i , we define (for $0 \leq i \leq L_{d2} - 1$):

$$\gamma_{2,k,i,m,n} = \exp(-Z_{2,k,i,m,n} / (2L_d \hat{\sigma}_w^2)) \quad (52)$$

where $Z_{2,k,i,m,n}$ is given by

$$\min_{\text{all } S_{m,n,1}} \sum_{n_r=1}^2 \left| \tilde{R}_{k,i,n_r} - \sum_{n_t=1}^2 \hat{H}_{k,i,n_r,n_t} S_{m,n,n_t} \right|^2 \quad (53)$$

Now, (50) and (52) are used in the forward and backward recursions of the BCJR algorithm [3].

G. Summary of the Receiver Algorithms

The receiver algorithms are summarized as follows:

- 1) Estimate the start-of-frame and the frequency offset (coarse) using (17), for each receive antenna. Obtain the average value of the frequency offset ($\hat{\omega}_k$) using (20).
- 2) Cancel the frequency offset by multiplying \tilde{r}_{k,n,n_r} in (15) by $e^{-j\hat{\omega}_k n}$, and estimate the channel using (27), for each n_r and n_t .
- 3) Obtain $\tilde{y}_{1,k,m,n_r,n_t}$ from (33) and the fine frequency offset using (34).
- 4) Cancel the frequency offset by multiplying \tilde{r}_{k,n,n_r} in (15) by $e^{-j(\hat{\omega}_k + \hat{\omega}_{k,f})n}$, and estimate the channel again using (27), for each n_r and n_t .
- 5) Obtain the average superfine frequency offset estimate using (44). Cancel the offset by multiplying \tilde{r}_{k,n,n_r} in (15) by $e^{-j(\hat{\omega}_k + \hat{\omega}_{k,f} + \hat{\omega}_{k,sf})n}$.
- 6) Obtain the noise variance estimate from (45).
- 7) Take the L_d -point FFT of $\tilde{r}_{k,m2,n_r}$ and perform turbo decoding.

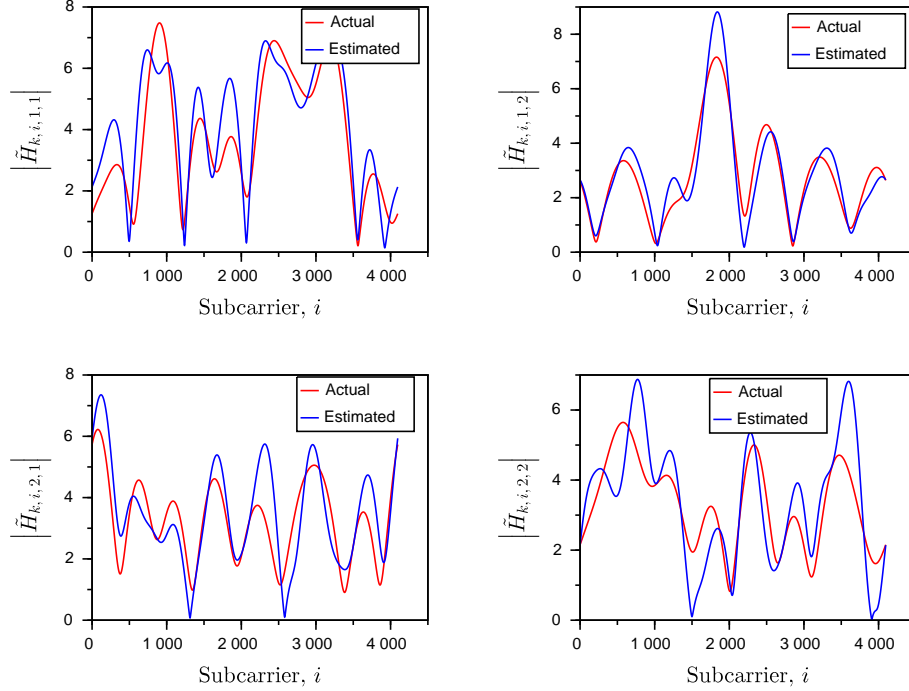


Figure 7. Magnitude spectrum of estimated and actual channel, $L_p = 512$.

H. Simulation Results

In this section, we present the simulation results for the proposed turbo coded MIMO OFDM system with $N_t = N_r = 2$. The SNR per bit is defined in (92). Note that one data bit (two coded QPSK symbols) is sent simultaneously from two transmit antennas. Hence, the number of data bits sent from each transmit antenna is $\kappa = 0.5$, as given in (92). We have also assumed that $\sigma_f^2 = 0.5$. The frame parameters are summarized in Table I. The maximum number of frames simulated is 2.2×10^4 , at an average SNR per bit of 6.5 dB. Each simulation run is over 10^3 frames. Hence, the maximum number of independently seeded simulation runs is 22.

TABLE I. FRAME PARAMETERS.

Parameter	Value (QPSK symbols)
L_p	512, 1024
L_d	4096
B	4
L_o	256, 512
L_{d2}	3832, 3576
L_h	10
$L_{cp} = L_{cs}$	18

The throughput is defined as [2] [3]:

$$\mathcal{T} = \frac{L_{d2}}{L_d + L_p + L_{cp} + L_{cs}}. \quad (54)$$

The throughput of various frame configurations is given in

TABLE II. THROUGHPUT.

L_p	L_o	L_{d2}	\mathcal{T}
512	256	3832	82.515%
1024	512	3576	69.356%

Table II. The BER simulation results for the turbo coded MIMO OFDM system with $N_t = N_r = 2$ is shown in Figure 10. Here “Id” denotes the ideal receiver. For the practical receivers (“Pr”), the interpolation factor for superfine frequency offset estimation is $I = 16$. The practical receiver with $L_p = 1024$, $L_o = 512$ attains a BER of 10^{-5} at an SNR per bit of 5.5 dB, which is 1 dB better than the receiver with $L_p = 512$, $L_o = 256$. This is due to the fact that the variance of the channel estimation error with $L_p = 512$ is twice that of $L_p = 1024$ (see (31)). This difference in the variance of the channel estimation error affects the turbo decoding process. Moreover, the practical receiver in Figure 10 with $L_p = 1024$, $L_o = 512$ is 2.5 dB better than the practical receiver with one transmit and two receive antennas in Figure 10 of [2].

TABLE III. PROBABILITY OF FRAME ERASURE.

Frame configuration	Probability of erasure
$L_p = 512$, $L_o = 256$	2.98×10^{-2}
$L_p = 1024$, $L_o = 512$	7×10^{-4}

The probability of frame erasure (this happens when (19)

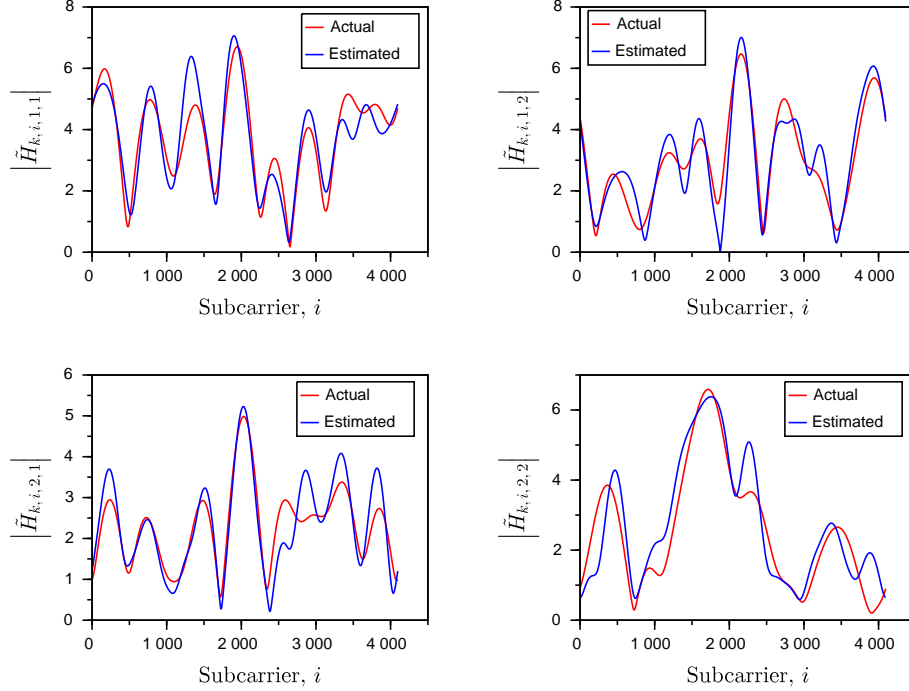


Figure 8. Magnitude spectrum of estimated and actual channel, $L_p = 1024$.

is not satisfied) at 0 dB SNR per bit is shown in Table III. Clearly, as L_p increases, the probability of erasure decreases. Finally, the root mean square (RMS) and maximum frequency offset estimation error in radians, at 0 dB SNR per bit, is given in Table IV.

IV. NEAR CAPACITY SIGNALING

In Sections II and III, we had presented the discrete-time algorithms for MIMO-OFDM. The inherent assumption in these two sections was that all transmit antennas use the same carrier frequency. The consequence of this assumption is that the signal at each receive antenna is a linear combination of the symbols from all the transmit antennas, as given in (46) and (48). This makes the estimation of symbols, $\mathbf{S}_{k,3,i}$ in (48), complicated for large values of N_t and N_r (massive MIMO). In this section, we assume that distinct transmit antennas use different carrier frequencies. Thus, the signals from distinct transmit antennas are orthogonal. To each transmit antenna, we associate N_r receive antennas, that are capable of receiving signals from one particular transmit antenna. The total number of receive antennas is now $N_r N_t$.

In order to restrict the transmitted signal spectrum, it is desirable to have a lowpass filter (LPF) at the output of the parallel-to-serial converter in Figure 3, for each transmit antenna. If we assume that the cut-off frequency of the LPF is $\pi/10$ radians and its transition bandwidth is $\pi/20$ radians, then the required length of the linear-phase, finite impulse response (FIR) LPF with Hamming window would be [48]

$$\begin{aligned} 8\pi/L_{\text{LPF}} &= \pi/20 \\ \Rightarrow L_{\text{LPF}} &= 160. \end{aligned} \quad (55)$$

Note that an infinite impulse response (IIR) filter could also be used. However, it may have stability problems when the cut-off frequency of the LPF is close to zero radians. If the physical channel has 10 taps as given by (3), then the length of the equivalent channel as seen by the receiver would be:

$$\begin{aligned} L_h &= L_{\text{LPF}} + 10 - 1 \\ &= 160 + 10 - 1 \\ &= 169. \end{aligned} \quad (56)$$

The values of L_p and L_d in Figure 1(a) have to be suitably increased to obtain a good estimate of the channel (see (31)) and maintain a high throughput (see 54). Let us denote the impulse response of the LPF by p_n . We assume that p_n is obtained by sampling the continuous-time impulse response $p(t)$ at a rate of $1/T_s$, where T_s is defined in (3). Note that p_n is real-valued [48]. The discrete-time Fourier transform (DTFT) of p_n is [17] [18]:

$$\begin{aligned} \tilde{P}_{\mathcal{P}}(F) &= \sum_{n=0}^{L_{\text{LPF}}-1} p_n e^{-j2\pi F n T_s} \\ &= \frac{1}{T_s} \sum_{m=-\infty}^{\infty} \tilde{P}(F - m/T_s) \end{aligned} \quad (57)$$

where the subscript \mathcal{P} denotes a periodic function, F denotes the frequency in Hz and $\tilde{P}(F)$ is the continuous-time Fourier transform of $p(t)$. Observe that:

- 1) the digital frequency ω in radians is given by
$$\omega = 2\pi F T_s \quad (58)$$
- 2) $\tilde{P}_{\mathcal{P}}(F)$ is periodic with period $1/T_s$

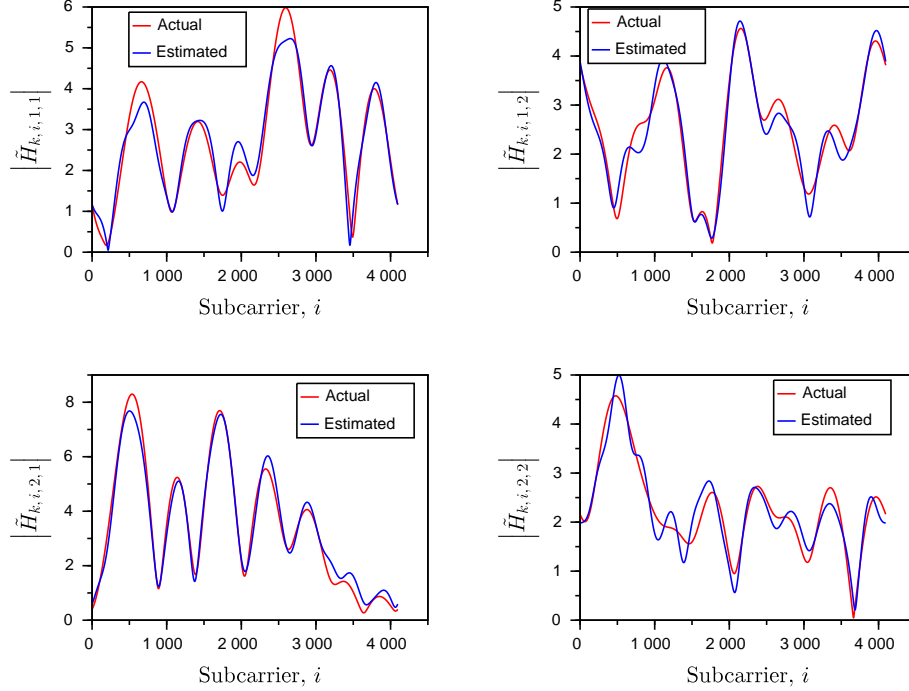


Figure 9. Magnitude spectrum of estimated and actual channel, $L_p = 4096$.

TABLE IV. FREQUENCY OFFSET ESTIMATION ERROR.

Frame configuration	Est. Error	Coarse	Fine	Superfine
$L_p = 512$ $L_o = 256$	RMS	1.71×10^{-3}	3.38×10^{-4}	5.85×10^{-5}
	Max.	2.4×10^{-2}	1.6×10^{-2}	2.6×10^{-4}
$L_p = 1024$ $L_o = 512$	RMS	3.3×10^{-4}	9.2×10^{-5}	4.3×10^{-5}
	Max.	1.2×10^{-2}	3.9×10^{-4}	1.82×10^{-4}

- 3) there is no aliasing in the second equation of (57), that is

$$\tilde{P}_{\mathcal{P}}(F) = \frac{\tilde{P}(F)}{T_s} \quad \text{for } -\frac{1}{2T_s} < F < \frac{1}{2T_s}. \quad (59)$$

Now, \tilde{s}_{k,n,n_t} in Figure 1(a) is passed through the LPF. Let us denote the LPF output by \tilde{v}_{k,n,n_t} . After digital-to-analog (D/A) conversion, the continuous-time signal is denoted by $\tilde{v}_{k,n_t}(t)$. The power spectral density of $\tilde{v}_{k,n_t}(t)$ [17] [18]

$$S_{\tilde{v}}(F) = \frac{1}{T_s} \cdot \frac{\sigma_s^2}{2} \cdot |\tilde{P}(F)|^2 \quad (60)$$

where we have assumed that the samples of \tilde{s}_{k,n,n_t} are uncorrelated with variance σ_s^2 given in (13). Thus the one-sided bandwidth of the complex baseband signal $\tilde{v}_{k,n_t}(t)$ is $1/(20T_s)$ Hz, for an LPF with cut-off frequency $\pi/10$ radians, since $1/T_s$ corresponds to 2π radians. Thus, the passband signal spectrum from a single transmit antenna would have a two-sided bandwidth of $1/(10T_s)$ Hz.

The frame structure is given by Figure 1. The average power of the preamble in the time domain must be equal to that of the data, as given by (13). Due to the use of different carrier frequencies for distinct transmit antennas, the same preamble pattern can be used for all the transmit antennas. Therefore, the subscript n_t can be dropped from the preamble signal, both in the time and frequency domain, in Figure 1(a) and (7). There are also no zero-valued preamble symbols in the frequency domain, that is [40]

$$S_{1,i} \in \sqrt{L_p/L_d} (\pm 1 \pm j) \quad (61)$$

for $0 \leq i \leq L_p - 1$. The block diagram of the system for near capacity signaling is shown in Figure 11. The received signal vector at the output of the FFT for the N_r antennas associated with the transmit antenna n_t , for the k^{th} frame and i^{th} ($0 \leq i \leq L_d - 1$) subcarrier is:

$$\tilde{\mathbf{R}}_{k,i,n_t} = \tilde{\mathbf{H}}_{k,i,n_t} S_{k,3,i,n_t} + \tilde{\mathbf{W}}_{k,i,n_t} \quad (62)$$

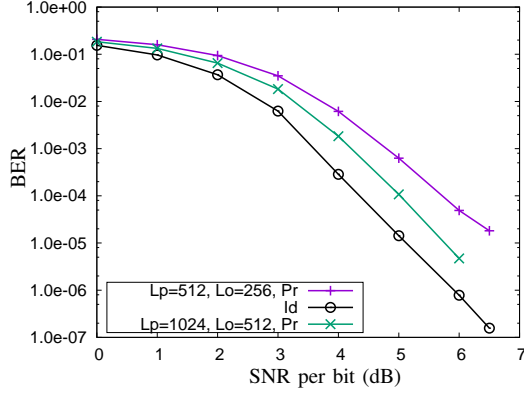


Figure 10. BER simulation results.

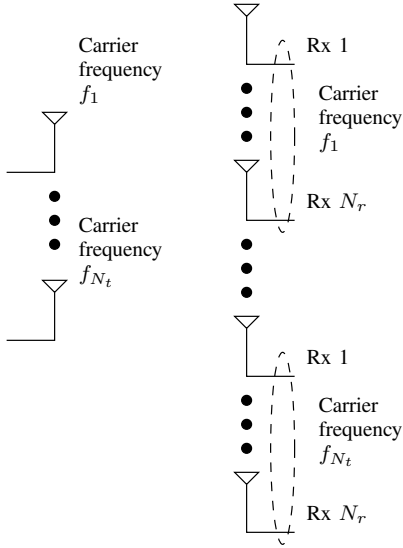


Figure 11. Near capacity signaling.

where $S_{k,3,i,n_t}$ is given in (7), $\tilde{\mathbf{R}}_{k,i,n_t}$, $\tilde{\mathbf{H}}_{k,i,n_t}$ and $\tilde{\mathbf{W}}_{k,i,n_t}$ are $N_r \times 1$ vectors given by:

$$\begin{aligned} \tilde{\mathbf{R}}_{k,i,n_t} &= \begin{bmatrix} \tilde{R}_{k,i,n_t,1} & \cdots & \tilde{R}_{k,i,n_t,N_r} \end{bmatrix}^T \\ \tilde{\mathbf{H}}_{k,i,n_t} &= \begin{bmatrix} \tilde{H}_{k,i,n_t,1} & \cdots & \tilde{H}_{k,i,n_t,N_r} \end{bmatrix}^T \\ \tilde{\mathbf{W}}_{k,i,n_t} &= \begin{bmatrix} \tilde{W}_{k,i,n_t,1} & \cdots & \tilde{W}_{k,i,n_t,N_r} \end{bmatrix}^T. \end{aligned} \quad (63)$$

Similar to (47), it can be shown that for $1 \leq l \leq N_r$

$$\begin{aligned} \frac{1}{2}E \left[\left| \tilde{W}_{k,i,n_t,l} \right|^2 \right] &= L_d \sigma_w^2 \\ \frac{1}{2}E \left[\left| \tilde{H}_{k,i,n_t,l} \right|^2 \right] &= L_h \sigma_f^2. \end{aligned} \quad (64)$$

The synchronization and channel estimation algorithms are identical to that given in Section III with $N_t = 1$.

In the turbo decoding operation we assume that $N_t = 2$. The generating matrix of the constituent encoders is given by

(49). For decoder 1 and $0 \leq i \leq L_{d2} - 1$, we define [2]:

$$\gamma_{1,k,i,m,n} = \prod_{l=1}^{N_r} \gamma_{1,k,i,m,n,l} \quad (65)$$

where

$$\gamma_{1,k,i,m,n,l} = \exp \left[- \frac{\left| \tilde{R}_{k,i,1,l} - \hat{H}_{k,i,1,l} S_{m,n} \right|^2}{2L_d \hat{\sigma}_w^2} \right] \quad (66)$$

where $\hat{\sigma}_w^2$ is the average estimate of the noise variance over all the N_r diversity arms, as given by (45) with $N_t = 1$, and $S_{m,n}$ is the QPSK symbol corresponding to the transition from state m to n in the encoder trellis. Similarly at decoder 2, for $0 \leq i \leq L_{d2} - 1$, we have:

$$\gamma_{2,k,i,m,n} = \prod_{l=1}^{N_r} \gamma_{2,k,i,m,n,l} \quad (67)$$

where

$$\gamma_{2,k,i,m,n,l} = \exp \left[- \frac{\left| \tilde{R}_{k,i,2,l} - \hat{H}_{k,i,2,l} S_{m,n} \right|^2}{2L_d \hat{\sigma}_w^2} \right]. \quad (68)$$

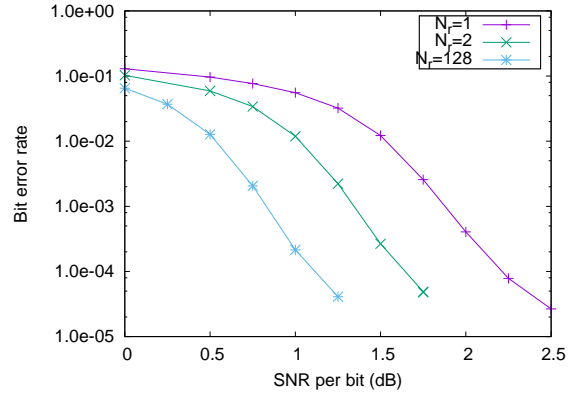


Figure 12. BER results for near capacity signaling with $N_t = 2$.

The simulation results assuming an ideal coherent receiver is given in Figure 12, for $L_d = 4096$, $L_p = L_o = B = L_{cp} = L_{cs} = 0$ (the preamble, postamble, buffer, cyclic prefix or suffix is not required, since this is an ideal coherent receiver), $N_t = 2$ and different values of N_r .

TABLE V. NUMBER OF SIMULATION RUNS FOR VARIOUS N_r .

N_r	SNR per bit (dB)	Max. no. of runs	Time for 1 run (minutes)
1	2.5	51	75
2	1.75	25	76
128	1.25	30	88

The maximum number of independently seeded simulation runs for various N_r and SNR per bit is given in Table V. For

lower values of the SNR per bit, the number of runs is less than the maximum. Each run is over 10^3 frames. The time taken for one run using Scilab on an i5 processor is also given in Table V. The total time taken to obtain Figure 12 is approximately three months. The channel coefficients $\tilde{H}_{k,i,n_t,l}$ in (63) are assumed to be complex Gaussian and independent over i and l , that is

$$\begin{aligned} \frac{1}{2}E \left[\tilde{H}_{k,i_1,n_t,l} \tilde{H}_{k,i_2,n_t,l}^* \right] &= L_h \sigma_f^2 \delta_K(i_1 - i_2) \\ \frac{1}{2}E \left[\tilde{H}_{k,i,n_t,l_1} \tilde{H}_{k,i,n_t,l_2}^* \right] &= L_h \sigma_f^2 \delta_K(l_1 - l_2). \end{aligned} \quad (69)$$

The average SNR per bit is given by the second equation in (92) with

$$\begin{aligned} P_{av} &= 2 \\ L_h \sigma_f^2 &= 0.5 \\ \kappa &= 0.5. \end{aligned} \quad (70)$$

The turbo decoder uses eight iterations. Observe that in Figure 12, we obtain a BER of 2×10^{-5} at an average SNR per bit of just 2.5 dB, for $N_r = 1$. It is also clear from Figure 12 that increasing N_r follows the law of diminishing returns. In fact there is only 1.25 dB difference in the average SNR per bit, between $N_r = 1$ and $N_r = 128$, at a BER of 2×10^{-5} . The slight change in slope at a BER of 2×10^{-5} is probably because the BER needs to be averaged over more number of simulation runs. We do not expect an ideal coherent detector to exhibit an error floor.

It is interesting to compare the average SNR per bit definitions given by (70) and (92) for $N_r = 1$ in this paper, with (38) in [40]. Observe that both definitions are identical. However, in Figure 12, we obtain a BER of 2×10^{-5} at an average SNR per bit of 2.5 dB, whereas in Figure 7 of [40] we obtain a similar BER at 8 dB average SNR per bit, for the ideal receiver. What could be the reason for this difference? Simply stated, in this section we have assumed a 4096-tap channel (see the first equation in (69) and equation (37) in [40] with $L_h = L_d$). However, in [40] we have considered a 10-tap channel. This is further explained below.

- 1) In this section, the SNR per bit for the k^{th} frame and $N_r = 1$ is proportional to (see also (22) in [2])

$$\text{SNR}_{k,\text{bit},1} \propto \frac{1}{L_d} \sum_{i=0}^{L_d-1} \left| \tilde{H}_{k,i,n_t,1} \right|^2 \quad (71)$$

where the subscript 1 in $\text{SNR}_{k,\text{bit},1}$ denotes case (1) and $\tilde{H}_{k,i,n_t,1}$ is defined in (63). Note that $\tilde{H}_{k,i,n_t,1}$ is a zero-mean Gaussian random variable which is independent over i and variance given by (64). Moreover, the right hand side of (71) gives the estimate of the variance of $\tilde{H}_{k,i,n_t,1}$. Let us now compute the variance of the estimate of the variance in (71), that is

$$\sigma_1^2 = E \left[\left(\frac{1}{L_d} \sum_{i=0}^{L_d-1} \left| \tilde{H}_{k,i,n_t,1} \right|^2 - 2L_h \sigma_f^2 \right)^2 \right] \quad (72)$$

where we have used (64). It can be shown that

$$\sigma_1^2 = \frac{\sigma_H^4}{L_d} = \frac{4L_h^2 \sigma_f^4}{L_d} \quad (73)$$

where for $0 \leq i \leq L_d - 1$

$$\begin{aligned} E \left[\left| \tilde{H}_{k,i,n_t,1} \right|^2 \right] &= 2L_h \sigma_f^2 && \triangleq \sigma_H^2 \\ H_{k,i,n_t,1,I} + j H_{k,i,n_t,1,Q} &= \tilde{H}_{k,i,n_t,1} \\ E \left[H_{k,i,n_t,1,I}^2 \right] &= \sigma_H^2 / 2 && \triangleq \sigma_{H,1}^2 \\ E \left[H_{k,i,n_t,1,Q}^2 \right] &= \sigma_H^2 / 2 && \triangleq \sigma_{H,1}^2 \\ E \left[H_{k,i,n_t,1,I}^4 \right] &= 3\sigma_{H,1}^4 \\ E \left[H_{k,i,n_t,1,Q}^4 \right] &= 3\sigma_{H,1}^4 \\ E \left[H_{k,i,n_t,1,I}^2 H_{k,j,n_t,1,I}^2 \right] &= \sigma_{H,1}^4 \quad i \neq j \\ E \left[H_{k,i,n_t,1,Q}^2 H_{k,j,n_t,1,Q}^2 \right] &= \sigma_{H,1}^4 \quad i \neq j \\ E \left[H_{k,i,n_t,1,I}^2 H_{k,j,n_t,1,Q}^2 \right] &= \sigma_{H,1}^4 \end{aligned} \quad (74)$$

where we have used the first equation in (69) and the assumption that $H_{k,i,n_t,1,I}$ and $H_{k,j,n_t,1,Q}$ are independent for all i, j .

- 2) Let us now compute the SNR per bit for each frame in [40]. Using the notation given in [40], we have

$$\text{SNR}_{k,\text{bit},2} \propto \frac{1}{L_d} \sum_{i=0}^{L_d-1} \left| \tilde{H}_{k,i} \right|^2 \quad (75)$$

where the subscript 2 in $\text{SNR}_{k,\text{bit},2}$ denotes case (2). Again, the variance of the estimate of the variance in the right hand side of (75) is

$$\sigma_2^2 = E \left[\left(\frac{1}{L_d} \sum_{i=0}^{L_d-1} \left| \tilde{H}_{k,i} \right|^2 - 2L_h \sigma_f^2 \right)^2 \right]. \quad (76)$$

Observe that $\tilde{H}_{k,i}$ in (76) is obtained by taking the L_d -point FFT of an L_h -tap channel, and the autocorrelation of $\tilde{H}_{k,i}$ is given by (37) in [40]. Using Parseval's theorem we have

$$\frac{1}{L_d} \sum_{i=0}^{L_d-1} \left| \tilde{H}_{k,i} \right|^2 = \sum_{n=0}^{L_h-1} \left| \tilde{h}_{k,n} \right|^2 \quad (77)$$

where $\tilde{h}_{k,n}$ denotes a sample of zero-mean Gaussian random variable with variance per dimension equal to σ_f^2 . Note that $\tilde{h}_{k,n}$ is independent over n (see also (1) in [40]). Substituting (77) and the first equation of (74) in (76) we get

$$\sigma_2^2 = E \left[\left(\sum_{n=0}^{L_h-1} \left| \tilde{h}_{k,n} \right|^2 - \sigma_H^2 \right)^2 \right]. \quad (78)$$

It can be shown that

$$\sigma_2^2 = 4L_h \sigma_f^4 \quad (79)$$

where we have used the following relations:

$$\begin{aligned}
E \left[\left| \tilde{h}_{k,n} \right|^2 \right] &= 2\sigma_f^2 \\
h_{k,n,I} + j h_{k,n,Q} &= \tilde{h}_{k,n} \\
E [h_{k,n,I}^2] &= \sigma_f^2 \\
E [h_{k,n,Q}^2] &= \sigma_f^2 \\
E [h_{k,n,I}^4] &= 3\sigma_f^4 \\
E [h_{k,n,Q}^4] &= 3\sigma_f^4 \\
E [h_{k,n,I}^2 h_{k,m,I}^2] &= \sigma_f^4 \quad n \neq m \\
E [h_{k,n,Q}^2 h_{k,m,Q}^2] &= \sigma_f^4 \quad n \neq m \\
E [h_{k,n,I}^2 h_{k,m,Q}^2] &= \sigma_f^4 \quad (80)
\end{aligned}$$

where we have assumed that $h_{k,n,I}$ and $h_{k,m,Q}$ are independent for all n, m .

Substituting

$$\begin{aligned}
L_h &= 10 \\
L_d &= 4096 \quad (81)
\end{aligned}$$

in (74) and (80) we obtain

$$\begin{aligned}
\sigma_1^2 &= 0.1\sigma_f^4 \\
\sigma_2^2 &= 40\sigma_f^4. \quad (82)
\end{aligned}$$

Thus we find that the variation in the SNR per bit for each frame is 400 times larger in case (2) than in case (1). Therefore, in case (2) there are many frames whose SNR per bit is much smaller than the average value given by (92), resulting in a large number of bit errors. Conversely, the average SNR per bit in case (2) needs to be much higher than in case (1) for the same BER.

V. CONCLUSIONS

Discrete-time algorithms for the coherent detection of turbo coded MIMO OFDM system are presented. Simulations results for a 2×2 turbo coded MIMO OFDM system indicate that a BER of 10^{-5} , is obtained at an SNR per bit of just 5.5 dB, which is a 2.5 dB improvement over the performance given in the literature. The minimum average SNR per bit for error-free transmission over fading channels is derived and shown to be equal to -1.6 dB, which is the same as that for the AWGN channel.

Finally, an ideal near capacity signaling is proposed, where each transmit antenna uses a different carrier frequency. Simulation results for the ideal coherent receiver show that it is possible to achieve a BER of 2×10^{-5} at an average SNR per bit equal to 2.5 dB, with two transmit and two receive antennas. When the number of receive antennas for each transmit antenna is increased to 128, the average SNR per bit required to attain a BER of 2×10^{-5} is 1.25 dB. The spectral efficiency of the proposed near capacity system is 1 bit/sec/Hz. Higher spectral efficiency can be obtained by increasing the number of transmit antennas with no loss in BER performance. A pulse shaping technique is also proposed to reduce the bandwidth of the transmitted signal.

Future work could address the issues of peak-to-average power ratio (PAPR).

APPENDIX

A. The Minimum Average SNR per bit for Error-free Transmission over Fading Channels

In this appendix, we derive the minimum average SNR per bit for error-free transmission over MIMO fading channels. Consider the signal

$$\tilde{r}_n = \tilde{x}_n + \tilde{w}_n \quad \text{for } 0 \leq n < N \quad (83)$$

where \tilde{x}_n is the transmitted signal (message) and \tilde{w}_n denotes samples of zero-mean noise, not necessarily Gaussian. All the terms in (83) are complex-valued or two-dimensional and are transmitted over one complex dimension. Here the term dimension refers to a communication link between the transmitter and the receiver carrying only real-valued signals. We also assume that \tilde{x}_n and \tilde{w}_n are ergodic random processes, that is, the time average statistics is equal to the ensemble average. The time-averaged signal power over two-dimensions is given by, for large values of N :

$$\frac{1}{N} \sum_{n=0}^{N-1} |\tilde{x}_n|^2 = P'_{av}. \quad (84)$$

The time-averaged noise power per dimension is

$$\frac{1}{2N} \sum_{n=0}^{N-1} |\tilde{w}_n|^2 = \sigma_w'^2 = \frac{1}{2N} \sum_{n=0}^{N-1} |\tilde{r}_n - \tilde{x}_n|^2. \quad (85)$$

The received signal power over two-dimensions is

$$\begin{aligned}
\frac{1}{N} \sum_{n=0}^{N-1} |\tilde{r}_n|^2 &= \frac{1}{N} \sum_{n=0}^{N-1} |\tilde{x}_n + \tilde{w}_n|^2 \\
&= \frac{1}{N} \sum_{n=0}^{N-1} |\tilde{x}_n|^2 + |\tilde{w}_n|^2 \\
&= P'_{av} + 2\sigma_w'^2 \\
&= E \left[|\tilde{x}_n + \tilde{w}_n|^2 \right] \quad (86)
\end{aligned}$$

where we have assumed independence between \tilde{x}_n and \tilde{w}_n and the fact that \tilde{w}_n has zero-mean. Note that in (86) it is necessary that either \tilde{x}_n or \tilde{w}_n or both, have zero-mean.

Next, we observe that (85) is the expression for a $2N$ -dimensional noise hypersphere with radius $\sigma_w' \sqrt{2N}$. Similarly, (86) is the expression for a $2N$ -dimensional received signal hypersphere with radius $\sqrt{N(P'_{av} + 2\sigma_w'^2)}$.

Now, the problem statement is: how many noise hyperspheres (messages) can fit into the received signal hypersphere, such that the noise hyperspheres do not overlap (reliable decoding), for a given N , P'_{av} and $\sigma_w'^2$? The solution lies in the volume of the two hyperspheres. Note that a $2N$ -dimensional hypersphere of radius R has a volume proportional to R^{2N} . Therefore, the number of possible messages is

$$M = \frac{\left(N (P'_{av} + 2\sigma_w'^2) \right)^N}{(2N\sigma_w'^2)^N} = \left(\frac{P'_{av} + 2\sigma_w'^2}{2\sigma_w'^2} \right)^N \quad (87)$$

over N samples (transmissions). The number of bits required to represent each message is $\log_2(M)$, over N transmissions.

Therefore, the number of bits per transmission, defined as the channel capacity, is given by [49]

$$\begin{aligned} C &= \frac{1}{N} \log_2(M) \\ &= \log_2 \left(1 + \frac{P'_{\text{av}}}{2\sigma_w'^2} \right) \quad \text{bits per transmission} \end{aligned} \quad (88)$$

over two dimensions or one complex dimension (here again the term “dimension” implies a communication link between the transmitter and receiver, carrying only real-valued signals. This is not to be confused with the $2N$ -dimensional hypersphere mentioned earlier or the M -dimensional orthogonal constellations in [18]).

Proposition A.1: Clearly, the channel capacity is additive over the number of dimensions. In other words, channel capacity over D dimensions, is equal to the sum of the capacities over each dimension, provided the information is independent across dimensions [2]. Independence of information also implies that, the bits transmitted over one dimension is not the interleaved version of the bits transmitted over any other dimension.

Proposition A.2: Conversely, if C bits per transmission are sent over $2N_r$ dimensions, (N_r complex dimensions), it seems reasonable to assume that each complex dimension receives C/N_r bits per transmission [2].

The reasoning for *Proposition A.2* is as follows. We assume that a “bit” denotes “information”. Now, if each of the N_r antennas (complex dimensions) receive the “same” C bits of information, then we might as well have only one antenna, since the other antennas are not yielding any additional information. On the other hand, if each of the N_r antennas receive “different” C bits of information, then we end up receiving more information (CN_r bits) than what we transmit (C bits), which is not possible. Therefore, we assume that each complex dimension receives C/N_r bits of “different” information.

Note that, when

$$\begin{aligned} \tilde{x}_n &= \sum_{n_t=1}^{N_t} \tilde{H}_{k, n, n_r, n_t} S_{k, 3, n, n_t} \\ \tilde{w}_n &= \tilde{W}_{k, n, n_r} \end{aligned} \quad (89)$$

as given in (46), the channel capacity remains the same as in (88). We now define the average SNR per bit for MIMO systems having N_t transmit and N_r receive antennas. We assume that κ information bits are transmitted simultaneously from each transmit antenna. The amount of information received by each receive antenna is $\kappa N_t/N_r$ bits per transmission, over two dimensions (due to Proposition A.2). Assuming independent channel frequency response and symbols across different transmit antennas, the average SNR of \tilde{R}_{k, i, n_r} in (46) can be computed from (47) as:

$$\text{SNR}_{\text{av}} = \frac{2L_h\sigma_f^2 P_{\text{av}} N_t}{2L_d\sigma_w'^2} = \frac{P'_{\text{av}}}{2\sigma_w'^2} \quad (90)$$

for $\kappa N_t/N_r$ bits, where

$$P_{\text{av}} = E \left[|S_{k, 3, i, n_t}|^2 \right]. \quad (91)$$

The average SNR per bit is

$$\begin{aligned} \text{SNR}_{\text{av}, b} &= \frac{2L_h\sigma_f^2 P_{\text{av}} N_t}{2L_d\sigma_w'^2} \cdot \frac{N_r}{\kappa N_t} \\ &= \frac{L_h\sigma_f^2 P_{\text{av}} N_r}{L_d\sigma_w'^2 \kappa} \\ &= \frac{P'_{\text{av}}}{2\sigma_w'^2} \cdot \frac{N_r}{\kappa N_t}. \end{aligned} \quad (92)$$

Moreover, for each receive antenna we have

$$C = \kappa N_t/N_r \quad \text{bits per transmission} \quad (93)$$

over two dimensions. Substituting (92) and (93) in (88) we get

$$\begin{aligned} C &= \log_2(1 + C \cdot \text{SNR}_{\text{av}, b}) \\ \Rightarrow \text{SNR}_{\text{av}, b} &= \frac{2^C - 1}{C}. \end{aligned} \quad (94)$$

Clearly as $C \rightarrow 0$, $\text{SNR}_{\text{av}, b} \rightarrow \ln(2)$, which is the minimum SNR required for error-free transmission over MIMO fading channels.

REFERENCES

- [1] K. Vasudevan, “Coherent turbo coded mimo ofdm,” in ICWMC 2016, The 12th International Conference on Wireless and Mobile Communications, Nov. 2016, pp. 91–99, [Online].
- [2] —, “Coherent detection of turbo-coded ofdm signals transmitted through frequency selective rayleigh fading channels with receiver diversity and increased throughput,” *Wireless Personal Communications*, vol. 82, no. 3, 2015, pp. 1623–1642. [Online]. Available: <http://dx.doi.org/10.1007/s11277-015-2303-8>
- [3] —, “Coherent detection of turbo-coded OFDM signals transmitted through frequency selective rayleigh fading channels with receiver diversity and increased throughput,” *CoRR*, vol. abs/1511.00776, 2015. [Online]. Available: <http://arxiv.org/abs/1511.00776>
- [4] J. G. Andrews et al., “What will 5g be?” *IEEE Journal on Selected Areas in Communications*, vol. 32, no. 6, June 2014, pp. 1065–1082.
- [5] O. Galinina, A. Pyattaev, S. Andreev, M. Dohler, and Y. Koucheryavy, “5g multi-rat lte-wifi ultra-dense small cells: Performance dynamics, architecture, and trends,” *IEEE Journal on Selected Areas in Communications*, vol. 33, no. 6, June 2015, pp. 1224–1240.
- [6] C. L. I et al., “New paradigm of 5g wireless internet,” *IEEE Journal on Selected Areas in Communications*, vol. 34, no. 3, Mar. 2016, pp. 474–482.
- [7] M. Agiwal, A. Roy, and N. Saxena, “Next generation 5g wireless networks: A comprehensive survey,” *IEEE Communications Surveys Tutorials*, vol. 18, no. 3, thirdquarter 2016, pp. 1617–1655.
- [8] F. Rusek et al., “Scaling up mimo: Opportunities and challenges with very large arrays,” *IEEE Signal Processing Magazine*, vol. 30, no. 1, Jan. 2013, pp. 40–60.
- [9] J. Hoydis, S. ten Brink, and M. Debbah, “Massive mimo in the ul/dl of cellular networks: How many antennas do we need?” *IEEE Journal on Selected Areas in Communications*, vol. 31, no. 2, Feb. 2013, pp. 160–171.
- [10] E. Bjrnson, E. G. Larsson, and M. Debbah, “Massive mimo for maximal spectral efficiency: How many users and pilots should be allocated?” *IEEE Transactions on Wireless Communications*, vol. 15, no. 2, Feb. 2016, pp. 1293–1308.
- [11] K. L. Wong, C. Y. Tsai, J. Y. Lu, D. M. Chian, and W. Y. Li, “Compact eight mimo antennas for 5g smartphones and their mimo capacity verification,” in 2016 URSI Asia-Pacific Radio Science Conference (URSI AP-RASC), Aug. 2016, pp. 1054–1056.
- [12] Z. Pi and F. Khan, “An introduction to millimeter-wave mobile broadband systems,” *IEEE Communications Magazine*, vol. 49, no. 6, June 2011, pp. 101–107.

- [13] T. S. Rappaport et al., "Broadband millimeter-wave propagation measurements and models using adaptive-beam antennas for outdoor urban cellular communications," *IEEE Transactions on Antennas and Propagation*, vol. 61, no. 4, Apr. 2013, pp. 1850–1859.
- [14] —, "Millimeter wave mobile communications for 5g cellular: It will work!" *IEEE Access*, vol. 1, 2013, pp. 335–349.
- [15] T. S. Rappaport, W. Roh, and K. Cheun, "Mobile's millimeter-wave makeover," *IEEE Spectrum*, vol. 51, no. 9, Sept. 2014, pp. 34–58.
- [16] S. Niknam, A. A. Nasir, H. Mehrpouyan, and B. Natarajan, "A multi-band ofdma heterogeneous network for millimeter wave 5g wireless applications," *IEEE Access*, vol. 4, 2016, pp. 5640–5648.
- [17] K. Vasudevan, *Digital Communications and Signal Processing*, Second edition (CDROM included). Universities Press (India), Hyderabad, www.universitiespress.com, 2010.
- [18] —, "Digital Communications and Signal Processing, Third edition," 2016, URL: <http://home.iitk.ac.in/~vasu/book0.pdf> [accessed: 2017-02-01].
- [19] N. Khalid and O. B. Akan, "Wideband thz communication channel measurements for 5g indoor wireless networks," in 2016 IEEE International Conference on Communications (ICC), May 2016, pp. 1–6.
- [20] N. R. Zulkefly et al., "Channel characterization for indoor environment at 17 ghz for 5g communications," in 2015 IEEE 12th Malaysia International Conference on Communications (MICC), Nov. 2015, pp. 241–245.
- [21] Q. Guo, G. Gui, and F. Li, "Block-partition sparse channel estimation for spatially correlated massive mimo systems," in 2016 8th International Conference on Wireless Communications Signal Processing (WCSP), Oct. 2016, pp. 1–4.
- [22] M. Kuerbis, N. M. Balasubramanya, L. Lampe, and A. Lampe, "On the use of channel models and channel estimation techniques for massive mimo systems," in 2016 24th European Signal Processing Conference (EUSIPCO), Aug. 2016, pp. 823–827.
- [23] V. Sridhar, T. Gabillard, and A. Manikas, "Spatiotemporal-mimo channel estimator and beamformer for 5g," *IEEE Transactions on Wireless Communications*, vol. 15, no. 12, Dec. 2016, pp. 8025–8038.
- [24] H. Xie, F. Gao, and S. Jin, "An overview of low-rank channel estimation for massive mimo systems," *IEEE Access*, vol. 4, 2016, pp. 7313–7321.
- [25] Q. Wang, Z. Zhou, J. Fang, and Z. Chen, "Compressive channel estimation for millimeter wave multiuser mimo systems via pilot reuse," in 2016 8th International Conference on Wireless Communications Signal Processing (WCSP), Oct. 2016, pp. 1–6.
- [26] B. Farhang-Boroujeny, "Ofdm versus filter bank multicarrier," *IEEE Signal Processing Magazine*, vol. 28, no. 3, May 2011, pp. 92–112.
- [27] Y. Chen, F. Schaich, and T. Wild, "Multiple access and waveforms for 5g: Idma and universal filtered multi-carrier," in 2014 IEEE 79th Vehicular Technology Conference (VTC Spring), May 2014, pp. 1–5.
- [28] B. Farhang-Boroujeny and H. Moradi, "Ofdm inspired waveforms for 5g," *IEEE Communications Surveys Tutorials*, vol. 18, no. 4, Fourthquarter 2016, pp. 2474–2492.
- [29] E. Basar, "Index modulation techniques for 5g wireless networks," *IEEE Communications Magazine*, vol. 54, no. 7, July 2016, pp. 168–175.
- [30] S. Venkatesan and R. A. Valenzuela, "Ofdm for 5g: Cyclic prefix versus zero postfix, and filtering versus windowing," in 2016 IEEE International Conference on Communications (ICC), May 2016, pp. 1–5.
- [31] P. Weitkemper et al., "Hardware experiments on multi-carrier waveforms for 5g," in 2016 IEEE Wireless Communications and Networking Conference, April 2016, pp. 1–6.
- [32] Z. Hraiech, F. Abdelkefi, and M. Siala, "Pops-ofdm with different tx/rx pulse shape durations for 5g systems," in 2015 5th International Conference on Communications and Networking (COMNET), Nov. 2015, pp. 1–6.
- [33] X. Zhang, L. Chen, J. Qiu, and J. Abdoli, "On the waveform for 5g," *IEEE Communications Magazine*, vol. 54, no. 11, Nov. 2016, pp. 74–80.
- [34] A. A. Zaidi et al., "Waveform and numerology to support 5g services and requirements," *IEEE Communications Magazine*, vol. 54, no. 11, Nov. 2016, pp. 90–98.
- [35] G. Berardinelli, K. I. Pedersen, T. B. Sorensen, and P. Mogensen, "Generalized dft-spread-ofdm as 5g waveform," *IEEE Communications Magazine*, vol. 54, no. 11, Nov. 2016, pp. 99–105.
- [36] C. An, B. Kim, and H. G. Ryu, "Design of w-ofdm and nonlinear performance comparison for 5g waveform," in 2016 International Conference on Information and Communication Technology Convergence (ICTC), Oct. 2016, pp. 1006–1009.
- [37] Y. Qi and M. Al-Imari, "An enabling waveform for 5g – qam-fbmc: Initial analysis," in 2016 IEEE Conference on Standards for Communications and Networking (CSCN), Oct. 2016, pp. 1–6.
- [38] R. Garzn-Bohrquez, C. A. Nour, and C. Douillard, "Improving turbo codes for 5g with parity puncture-constrained interleavers," in 2016 9th International Symposium on Turbo Codes and Iterative Information Processing (ISTC), Sept. 2016, pp. 151–155.
- [39] L. Guo, Z. Ning, Q. Song, Y. Cui, and Z. Chen, "Toward efficient 5g transmission: Ser performance analysis for asynchronous physical-layer network coding," *IEEE Access*, vol. 4, 2016, pp. 5083–5097.
- [40] K. Vasudevan, "Coherent detection of turbo coded ofdm signals transmitted through frequency selective rayleigh fading channels," in *Signal Processing, Computing and Control (ISPC), 2013 IEEE International Conference on*, Sept. 2013, pp. 1–6.
- [41] A. Goldsmith, S. A. Jafar, N. Jindal, and S. Vishwanath, "Capacity limits of mimo channels," *IEEE Journal on Selected Areas in Communications*, vol. 21, no. 5, June 2003, pp. 684–702.
- [42] Y. Wang and D. W. Yue, "Capacity of mimo rayleigh fading channels in the presence of interference and receive correlation," *IEEE Transactions on Vehicular Technology*, vol. 58, no. 8, Oct. 2009, pp. 4398–4405.
- [43] F. Benkhelifa, A. Tall, Z. Rezeki, and M. S. Alouini, "On the low snr capacity of mimo fading channels with imperfect channel state information," *IEEE Transactions on Communications*, vol. 62, no. 6, June 2014, pp. 1921–1930.
- [44] K. Vasudevan, "Iterative Detection of Turbo Coded Offset QPSK in the Presence of Frequency and Clock Offsets and AWGN," *Signal, Image and Video Processing*, Springer, vol. 6, no. 4, Nov. 2012, pp. 557–567.
- [45] —, "Design and development of a burst acquisition system for geosynchronous satcom channels," *CoRR*, vol. abs/1510.07106, 2015. [Online]. Available: <http://arxiv.org/abs/1510.07106>
- [46] H. Minn, V. K. Bhargava, and K. B. Letaief, "A Robust Timing and Frequency Synchronization for OFDM Systems," *IEEE Trans. on Wireless Commun.*, vol. 2, no. 4, July 2003, pp. 822–839.
- [47] S. Haykin, *Adaptive Filter Theory*, 3rd ed. Prentice Hall, 1996.
- [48] J. G. Proakis and D. G. Manolakis, *Digital Signal Processing: Principles, Algorithms and Applications*, 2nd ed. Maxwell MacMillan, 1992.
- [49] J. G. Proakis and M. Salehi, *Fundamentals of Communication Systems*. Pearson Education Inc., 2005.